BNL-NUREG-63326

MODELING OF TWO-PHASE FLOW INSTABILITIES DURING STARTUP TRANSIENTS UTILIZING RAMONA-4B METHODOLOGY*

CONF-961105--14

J. PANIAGUA, U.S. ROHATGI [1], and V. PRASAD
State University of New York at Stony Brook
College of Engineering and Applied Science
Stony Brook, New York 11794-2300

RAMONA-4B code is currently under development for simulating thermal hydraulic instabilities that can occur in Boiling Water Reactors (BWRs) and the Simplified Boiling Water Reactor (SBWR). As one of the missions of RAMONA-4B is to simulate SBWR startup transients, where geysering or condensation-induced instability may be encountered, the code needs to be assessed for this application. This paper outlines the results of the assessments of the current version of RAMONA-4B and the modifications necessary for simulating the geysering or condensation-induced instability. The test selected for assessment are the geysering tests performed by Prof. Aritomi (1993).

1. INTRODUCTION

The current Light Water Reactors achieve shutdown through active safety systems. Passive safety systems have been proposed for advanced designs to enhance the reliability of safety functions. The natural circulation Simplified Boiling Water Reactor (SBWR) by General Electric has been proposed as one such concept. Because natural circulation systems require power to initiate the natural circulation through void generation, thereby coupling the flow to the power, thermal hydraulic instabilities have been experienced under low pressure conditions, in such systems. If such instabilities were to transpire in the natural circulation SBWR during startup, the startup operations would experience difficulties because void fraction fluctuations in the reactor core would lead to power oscillations due to strong void reactivity feedback in the core. Therefore, it is deemed necessary to investigate and understand properly the thermal hydraulic instabilities during startup.

Recently, some concerns have been raised about the possibility of geysering or condensation-induced instability during startup from low pressure and low flow conditions in a natural circulation plant like the SBWR (Aritomi, 1992). Aritomi (1990, 1991, 1992, 1993) and Chiang (1992) have conducted extensive research in the area of geysering under natural circulation. In addition, F. Ineda and Y. Yasuo (1992) and Masuhara, et. al. (1993) have also performed small scale experiments to demonstrate this phenomenon. These experiments illustrated that the geysering-mode oscillations could occur at low pressures and low flows under certain thermal hydraulic conditions. Aritomi, et. al. (1992) explained the driving mechanism of geysering as follows: when voids are generated in a heated channel, a large slug of bubble forms, which grows due to decrease in hydrostatic pressure head as it moves toward the exit. The vapor then mixes with the liquid in the subcooled riser or upper plenum and is condensed there. Due to the bubble collapse and subsequent decrease in pressure, the subcooled liquid reenters the channel and restores the non-boiling condition. This process repeats periodically causing flow oscillations. It is evident then that bubble formation, growth, and collapse phenomena are of importance to the geysering instability.

1.1 Objective

The objective of this assessment is to determine the following:
(1) Whether the RAMONA methodology can simulate the geysering-type or condensation-induced instability encountered during startup in natural circulation systems.
(2) If not, what modifications are needed to qualitatively reproduce the instability.

2.0 RAMONA-4B METHODOLOGY

The RAMONA-4B code is designed to predict the three-dimensional neutron kinetics parameters in the reactor core, the thermal hydraulic parameters in the pressure vessel, and the recirculation loops and steam lines of SBWR's as it operates under steady-state or transient conditions. It uses

---

[1] *Brookhaven National Laboratory, Upton, NY 11973*
* *Partially supported by USNRC*

nonhomogeneous, nonequilibrium two-phase flow formulation. The drift flux model is utilized to obtain the relationship between the phasic velocities. The void, moderator and Doppler reactivity feedbacks are used to couple the neutronics to the core thermal hydraulic calculations. In the analysis of the SBWR, this feature is essential, since the buoyancy-induced core flow rate is strongly coupled to core thermal power. Flow increases as power is increased in the core. Stability limits are expressed by the power-to-flow ratio in the core.

The RAMONA-4B code strength is the computational speed without compromising the accuracy. Assumption of a single system pressure and momentum integral approach leads to benefits such as computational speed enhancement. However, these same assumptions also place some limitations on the capability of the code to model geysering instability. Among the important assumptions is the single system pressure for all thermo-physical property calculations. This assumption also permits the integration of the momentum equation separately from the mass and energy equations since it effectively decouples the balance equations. A brief description of RAMONA-4B is given in Appendix A.

3.0 DESCRIPTION OF TEST

Figure 1 shows a schematic diagram of Aritomi's test loop (Chiang, 1992). The loop is operated at atmospheric conditions with water as the test fluid. Heat fluxes up to 800 kW/m^2 were utilized in these experiments. Based on heater rod geometry and a heat flux of 100 kw/m^2, total power is 3.762 kw. This represents the heat flux upper limit where the geysering instability was observed (Chiang, 1992). Figure 2 is an illustration of the heated test section with the dimensions (Chiang, 1992). The test section consists of two parallel channels, each with a central heater rod between the inlet and outlet plena. Total flow rate was measured by an orifice flowmeter. Circulating fluid temperature was regulated by precoolers and preheaters installed in a separator tank. Steam generated in the test section was condensed in a condenser attached in the separator. Each channel consisted of a heater, two electrodes, and an orifice flowmeter for measuring flow oscillations. Differential pressures between the inlet and outlet plenums and between the plenums and steam separator were measured with differential pressure transducers and recorded with a transient digital recorder. Temperatures in the inlet plenum and separator were measured with another digital recorder. Tests were run at natural circulation conditions with constant inlet velocity. For natural circulation tests, the flow increased as the power increased. Figure 3 depicts the transient phenomenon in four steps as shown (Aritomi, 1993). The output experimental data shown highlights the oscillatory behavior of geysering. These experiments illustrated the thermal hydraulic features of geysering and they are:

(1) Flow oscillations appear with a phase difference of 180 degrees between the two channels.

(2) Flow reversal occurs in turn in both channels.

(3) Frequency of the natural circulation flow oscillation is twice the flow oscillation in each channel.

Requirements for geysering at startup include subcooled boiling and low pressure conditions, subcooled liquid in the upper plenum, and large bubbles or voids in the parallel channels. Although oscillations have been demonstrated in these experiments, the two recent startups of the Dodewaard reactor during 1992 did not exhibit any instability according to Nissen (1992). However, there are sufficient differences between the laboratory experiments and the Dodewaard reactor that results and conclusions from the experimental tests can not be made directly applicable to the SBWR design. Geysering appearing in parallel channels under natural circulation conditions is not as well understood as the density-wave oscillation instability. Sufficient basic design information is not available to prevent it from occurring.

4.0 MODELLING WITH RAMONA-4B CODE

The objective of the assessment of the RAMONA-4B code for geysering prediction is to validate whether or not the code in its current version has the capability to predict the geysering instability at startup. The basis of the assessment will be Aritomi's experimental test setup as shown in Figures 1 & 2. The computational results from RAMONA-4B will be compared from documented data of Aritomi's test to assess the code capability.

RAMONA-4B has been used to model Aritomi's test (1993). Figure 4 is a schematic of the nodalization for the test facility loop for Aritomi's experiment (1993). The input model consists of a total of 78 nodes and contains two heated parallel channels connected to inlet and outlet plenums. The model also includes a downcomer section which completes the flow loop. Table I shows the geometric parameters and nodalization scheme of the RAMONA-4B input deck used to simulate Aritomi's experiment. The system pressure is 1 bar and core inlet temperature is 90 °C. The heat flux input into the computer model is a step-change input initiated at the start of the simulation.

5.0 RESULTS

Assessment of the geysering-induced instability as predicted by RAMONA-4B is discussed here. Two separate cases were simulated with this model configuration. In the first case, the two parallel channels had equal and axially uniform heating. The initial power was 1 W per channel. Pressure was atmospheric with a core inlet subcooling of 10 °C. In the second case, one of the channels had a slightly lower power of 0.999 W to create asymmetric heating between the parallel channels. Core subcooling and pressure conditions were identical to the first case.

Results from the computational simulation for the uniform power distribution case revealed condensation-induced flow

DISCLAIMER

oscillations in the parallel channels. Since the channel power distributions are identical to each other respectively, this configuration is equivalent to a single channel model where the total initial heating in the channel is 2 W. Results are illustrated in Figures 5 through 6. At time t = 0, the power was ramped as a step-change input from 1 W in each channel to 1.886 kW in each for a total power of 3.762 kW in the test section. Total power in Aritomi's test was estimated from the heater rod geometry from the maximum heat flux of 100 kW/m^2 utilized in the experiment. Figure 5 displays channel 1 & channel 2 and total core flow behavior with the given power step input change. Flow oscillates with a period of approximately 6.5 seconds or a frequency of 0.15 Hz. Voids initially form at the top of the heated section of the channels and then propagate downward towards the channel inlets. Figure 6 shows the average void fraction for the core or two parallel channels. The limit cycle core average void fraction is shown to be approximately 0.19. The results reveal that the flow oscillations are due to the condensation or collapse of void in the subcooled upper plenum. Table 2 shows evaporation/condensation rates in various cells of the channel and riser (where the upper plenum is situated) for various times throughout the transient. Positive values indicate evaporation whereas negative values represent condensation. Note, the increase in core flow at t = 4 seconds as shown in Figure 5. This is due to the condensation taking place at the entrance of the riser as shown in Table 2. Comparing the condensation rate in the riser inlet cell with the exit cells of each of the heated channels, the condensation rate in the riser cell is considerably greater. Condensation is taking place in the exit cells of the channels because they are unheated. However, due to the smaller thermal mass in each of these channel exit cells, the temperature of the liquid increases at a faster rate than in the riser cells. Therefore, less condensation take place in the channel exit cells as compared to the riser inlet cell. The void collapse due to condensation in the riser cell then creates a low pressure situation which induces sudden increases of flow of subcooled liquid at the inlet of the channel. Because this riser cell is shared by both channels due to the computational formulation of RAMONA-4B, this effect is also shared by both the channels which explains the in-phase oscillations between the channels. Thus the subcooled conditions are restored in the channels as in geysering as shown in Figure 6. This cycling would continue until the amount of subcooling in the upper plenum/riser is insufficient to maintain the condensation rates that cause the oscillations. However, due to the uniform symmetry of the channels in the test section, out-of-phase oscillations between the channels did not occur as was observed in the Aritomi's experiment. The out-of-phase behavior was not expected in the calculation since the model configuration is equivalent to a single channel model configuration and no asymmetric heating was introduced to either of heated channels. This is illustrated by the equal flow distributions in each channel as shown in Figure 5.

The results for the asymmetrically heated case are displayed in Figures 7-9. Again, oscillatory behavior is seen in the channels for the flow and void fraction. As seen in Figures 7 through 9, the channel 1 inlet flow oscillates with a period of approximately 6.0 seconds, or a frequency of 0.16 Hz. This is slightly higher than the previous case of symmetric power distribution between the channels. In addition, the inlet flows for channels 1 and 2 undergo oscillations which are out-of-phase by 180 degrees. Figure 8 shows the total core inlet flow oscillation with a period of 3 seconds or a frequency of approximately 0.33 Hz. This indicates the frequency of the natural circulation oscillation to be twice the flow oscillation in each channel. Similarly, out-of-phase behavior is observed for two channels for exit flows as shown in Figure 8. Figure 9 shows that the core average void fraction to approach a limit cycle with a maximum of approximately 0.15. This is slightly lower than the symmetrically heated case due to the out-of-phase oscillations between the channels.

Analyzing the calculation results, we observe that the out-of-phase oscillations with a phase difference of 180 degrees between two channels and circulation loop oscillation frequency of twice that of the flow oscillation in each channel are the features of geysering or condensation-induced instability of two parallel channel tests. However, geysering experiments also observed out-of-phase flow reversal in the channels which was not predicted by the code. As noted earlier, condensation is taking place in the channel exits, however, the rate is not large enough to induce flow reversal in either of the channels. The out-of-phase oscillation and reverse flow will occur if the evaporation and subsequent condensation rate in a channel, is greater than the overall loop flow rate of the system. The condensation rates in each of the individual channels are small due to the low exit cell subcooling. This is the result of the relatively small thermal mass in the channel exit cell compared to the riser inlet cell. Thus the liquid temperature increases at a greater rate in the channel exit cell than in the riser inlet cell leading to relatively higher subcooling in the riser inlet cell. As a result, the condensation rate in the riser inlet cell is much greater than the channel exit cell. However, as the channel exit cells share the same riser inlet cell, both channels would experience the same effect of large condensation rate occurring in the riser. Furthermore, as the predicted localized condensation rates in the channel exit cells did not exceed the overall loop circulation rate, the code did not predict out-of-phase flow reversal in either of the channels.

A modification to the RAMONA-4B is required to allow the condensation of vapor to take place locally at the channel exit and not in the upper plenum where the condensation effect is felt by both channels. These modifications to the code are discussed in the next section. Furthermore, the vapor generation and condensation rates were also increased to achieve flow reversal.

5.1 Modifications to RAMONA-4B Code

In this section, three sensitivity calculations are presented. These calculations include either change to the code or to the input description. In the first calculation the channel exit cells

were enlarged. In the second calculation the effect of enhanced vapor generation was tested. In the third calculation the combined effect of the first two changes were assessed.

The first modification recommended is to partition the riser inlet cell between the two channels. This will have the effect of increasing the thermal mass in each channel's exit cell. As a result, the rate of temperature rise is reduced and the large subcooling condition, required for large condensation rates, is maintained. The condensation would then become localized to each channel with the possibility of reverse flow occurring due to the condensation rate being greater than the overall loop flow rate in the system. Figure 10 depicts the modification to the nodalization. The cross-sectional areas of channel exit cells are enlarged to one-half the riser inlet cell cross-sectional area. This modification enlarges the exit cell volumes sufficiently to produce only a small increase in the temperature in the exit cells, thereby, maintaining the large subcooling, necessary for condensation-induced geysering instability. No heating takes place in these enlarged exit cells and the overall system geometry has been revised so as to be the equivalent to the base case system geometry that was simulated earlier.

The results are shown in Figures 11 through 14. When compared to the base case of the current version of RAMONA-4B (Figures 7-9), the outcomes are surprisingly similar. Condensation rates shown in Figure 14 are not large enough to induce flow reversal in either channel. Figure 13 shows that the core average void fraction, after the initial startup time of 30 seconds, stabilizes to a limit cycle peak value of approximately 0.15. The limit cycle peak value of the core average void fraction is comparable to the previous case shown in Figure 9. The channel void fraction could not be compared with Aritomi's test as the void fraction was not measured.

In the second modification, the bulk vapor generation model in the current version of RAMONA-4B was modified to increase the core average void fraction. The remaining model is the same as the base case, with no enlargement of the exit cells. As stated earlier, the vapor generation model in the code is an empirical model based on experimental test data at high pressure conditions. The validity of the curve-fit model for vapor generation needs to be ascertained for low-power, low-pressure startup conditions. For this sensitivity simulation, the coefficient C_{11} in bulk vapor generation term was increased from 5.0 E6 W/(m^3-C) to 5.0 E7 W/(m^3-C) (see Appendix A, Eq. 10). Figures 15 through 18 represent the results of this modification to the vapor generation. As seen in these figures, the results are essentially the same as the base case for the current version of RAMONA-4B. The limit cycle peak value of the core average void fraction is approximately 0.15 as shown in Figure 17. This is essentially the same results as the base case which did not incorporate the enhanced vapor generation model. The difference is in the initial thirty seconds of the transient where chaotic behavior appears. This can be explained as follows: large voids are generated in the channel due to low flow conditions and power step-change increase at the start of the transient. These void fractions (Figure 17) are larger than the RAMONA-4B base case void fractions (Figure 9) due to the vapor generation model enhancement. Because of initial low flow conditions in the channel, the subcooled liquid region is near the channel entrance. The large voids produce the buoyancy that drives the natural circulation of the system. There is a lag between power and flow due to the flow inertia of the system. The chaotic behavior is observed due to the loop flow adjusting to the specified power input with the buoyancy and flow inertia acting against one another. Once the overall loop flow has risen to match the power input, the system settles down to the orderly oscillatory behavior seen in the transient after t=30 seconds. As loop flow increases with time, the subcooled liquid region in the channel rises in the channel. The voids generated in the channel decrease in time towards a limit value as a result. This is illustrated in Figure 17. Therefore, the only consequence the vapor generation model enhancement has in the base case RAMONA-4B simulation is the initiation of chaotic behavior at the beginning of the transient. Table III highlights the condensation rates in the individual channel exit cells and the riser inlet cell for the enhanced vapor generation model utilizing the current version of RAMONA-4B. As noted before, because the exit cell volumes are small when compared to the riser inlet computational cell, the rate of temperature rise in these cells is greater than that in the riser cell. Therefore, the subcooling is relatively larger in the riser cell, which leads to larger condensation taking place at that location. Table III shows the condensation rate in riser inlet cell to be much greater than the condensation occurring in channel exit cells. Thus the condensation-induced effects are not localized to each channel. Rather, the void collapse in riser inlet cell is seen by both channels and flow reversal can not occur in either channel. However, the out-of-phase oscillations with a phase difference of 180 degrees, and the natural circulation frequency of twice the flow oscillation in either channel, were maintained.

In the third sensitivity calculation, the identical modification to the vapor generation model is made to the modified RAMONA-4B code with the enlarged channel exit cells as described for the first calculation, the results are strikingly different. Figure 19 displays the increased magnitude in amplitude to the channel inlet flows and exhibits the total core inlet flow rate. In addition, there are out-of-phase flow reversals in both channels which is a characteristic of the geysering or condensation-induced instability. Figure 20 displays the total core inlet flowrate.

The exit mass flow rate also experiences flow reversal as illustrated in Figure 21. This was also observed in Aritomi's tests (1990, 1992). The frequency of oscillatory core flow is twice that of the flow oscillation in each channel. The limit cycle peak value core average void fraction is approximately 0.35 as shown in Figure 22. This is substantially higher than any of the previous calculations. This can be attributed to the flow reversals occurring in either channel during the transient. Low velocities are encountered in the channel when switching from normal flow to reverse flow and vice-versa. As a result, more voids are generated in the channel because the channel

subcooling region moves towards the inlet due to the low inlet velocities. Consequently, the two-phase region in the channel is increased. The channel exit cell condensation rates are shown in Figure 23. Here, the condensation rates are much larger than in previous simulations and are larger enough to cause flow reversal in the channels. In addition, note, the out-of-phase condensation oscillations between the channels. Figure 24 represents the individual channel liquid inlet velocities which display the same oscillatory behavior as the channel inlet flow rates. Table IV indicates the condensation rates occurring at various times in the channel exit cells and the "split riser" inlet cells. The largest condensation rates occur in the "split riser" inlet cells which essentially localizes the effect to each channel. Thus, the three stated features of the geysering or condensation-induced instability are predicted in this modified version of RAMONA-4B with the "split riser" change and the enhanced vapor generation model.

It is interesting to observe the magnitude of the forward flows being approximately four times that of the reversed flows. This is because at the instant of flow reversal, the reversed flow is resisted by the downcomer pressure head at the same time flow is being heated in the heater region of the channels. Therefore, the buoyancy force generated against the reversed flow direction was reduced.

Table V is a summary of the results of each simulation using the current version of RAMONA-4B and the version incorporating the "split riser" modification.

5.2 Comparison With Experimental Data

As seen earlier, Figure 3 shows Aritomi's experimental data (1992, 1993). Displayed are the individual channel inlet flow velocities, total core inlet flow velocity, and pressure drop. These graphs show the essential characteristics of geysering; out-of-phase oscillations with a phase difference of 180 degrees between the channels, flow reversal in each channel, and the natural circulation frequency being twice that of the flow oscillations in each channel. In Aritomi's experimental data, the peak inlet velocity reaches approximately 0.70 m/sec. The period of these oscillations is 6 seconds which corresponds to a frequency of 0.16 Hz. The total core inlet velocity time period is 3 seconds with the frequency being 0.33 Hz or twice that of the individual channel flows. Comparing with the results from the modified RAMONA-4B with "split riser" and enhanced vapor generation model change, the periods or frequencies were found to be almost identical. However, the magnitude of the predicted channel inlet velocities (Figure 23) were almost three times that observed in Aritomi's test as shown in Figure 3. The possible reason for this discrepancy is that the enhanced vapor generation model overpredicts the vapor generation in the Aritomi's experiment. However, the objective of this study was to assess the capability of the code to predict this instability.

A breakdown of what is happening during each flow oscillation is described here. Sections of Figures 21 through 24, which represent channel 1's exit mass flow rate, core average void fraction, liquid inlet velocity, and exit condensation rate, respectively, have been presented in Figure 25, which will be used to explain events in the condensation-induced oscillation. The time period between 59 and 65 seconds is investigated for this chain of flow events. At approximately 59 seconds, large voids are generated in the channel as seen in Figure 25(d) with peak void amplitude occurring at about 60 seconds. When voids are first generated in the channel, flow reversal takes place at the channel inlet as depicted in Figure 25(b) due to the sudden vapor volumetric expansion in the heated portion of the channel. At the same time, Figure 25(a) shows the flow at the channel exit has also increased due to the volumetric expansion of the vapor in the channel. Large void fractions which formed earlier in the channel are now being condensed in the channel exit. Figure 25(c) displays the increase in condensation rate at the channel exit due to the increase in channel vapor generation. Peak channel exit condensation coincides with peak channel void fraction as shown respectively in Figures 25(c) and 25(d). After $t = 60$ seconds, the void fraction in the channel decreases due to the increase in subcooled inlet flow. However, due to flow inertia, the peak amplitude of the channel inlet flow in Figure 25(b) does not occur until approximately 60.5 seconds, a one-half second lag. In addition, at this time, the large voids generated in the channel have moved up to the exit and condensed there as shown in Figure 25(c). The channel inlet flow then begins to decrease due to the decreased buoyancy in the channel as the subcooling condition is restored as shown in Figure 25(e). At the same time, vapor is being generated in channel 2 as illustrated in Figure 25(f) at approximately $t = 62$ seconds. Therefore, the vapor generation is out-of-phase between the channels. The expulsion of liquid or flow reversal at the inlet of channel 2 due to vapor generation causes a temporary increase or flow "spike" in channel 1 as shown in Figure 25(b) at $t = 62$ seconds. However, after this flow "spike", the channel 1 inlet flow continues decreasing due to the decreasing buoyancy in the channel. Peak amplitude of void fraction in channel 2 occurs at approximately $t = 63$ seconds as noted in Figure 25(f). In addition, peak condensation at channel 2 exit occurs at this time. Because of this large condensation taking place at channel 2's exit, flow reversal occurs at channel 1's inlet. This is due to the condensation rate being greater than the natural circulation rate of the system. After $t = 63$ seconds when flow reversal occurred in channel 1, the inlet flow begins to increase again due to the subcooled liquid being heated in the channel. The subcooled condition in channel 2 is restored at $t = 64$ seconds. At approximately $t = 65$ seconds the oscillatory flow cycle is repeated again as flow reversal occurs at channel 1's inlet due to the sudden generation of vapor in the channel. The flow cycle history is identical for channel 2. Figure 26 depicts graphically the set of events described above occurring for channel 1's inlet flow.

6.0 CONCLUSIONS

RAMONA-4B code was able to simulate out-of-phase

oscillations characteristic of the geysering or condensation induced instability. However, flow reversal in either channel cannot be predicted in the current version of RAMONA-4B. The modification to RAMONA-4B incorporating a "split riser" allows the code to qualitatively simulate flow reversals in either channel and out-of-phase oscillations which are features of this thermal hydraulic instability. However, it must be noted that the bulk vapor generation model required revision to achieve the flow reversals. By adjusting one of the empirical coefficients, the bulk vapor generation was increased in the channel which influenced the geysering instability. The amplitude of the calculated oscillations were greater than the experimental ones by a factor of three. This implies that the vapor generation was enhanced more than needed. The quantitative comparison between the experimental data and these computational runs indicates the bulk vapor generation model needs further improvement. As stated earlier, the vapor generation model is an empirical model based on experimental test data where the system pressures were considerably higher than the low-pressure conditions that occur during startup. The validity of the curve-fit model for vapor generation needs to be ascertained for low-power, low-pressure startup conditions.

REFERENCES

Aritomi, M., Chiang, J.H., Mori, M., "Geysering in Parallel Boiling Channels", Nuc. Engrg. and Des. 141, North Holland, Amsterdam (1993), 111-121.

Aritomi, M., et. al., "Fundamental Study on Thermo-Hydraulics during Startup in Natural Circulation Boiling Water Reactors, (I)", J. of Nuclear Science and Technology, 29-7, 1992, 631-641.

Aritomi, M., Chiang J.H., and Mori, M., "Transient Behavior of Natural Circulation for Boiling Two-Phase Flow (2nd Report, Mechanism of Geysering)", Proc. 1st JSME/ASME Joint Int. Conf. Nucl. Eng., Tokyo, Japan, 357, November 1991.

Aritomi, M., Nakahashi, T., Chiang, J.H., Wataru M., and Mori, M., "Transient Behavior of Natural Circulation for Boiling Two-Phase Flow (Experimental Results)", 6th Proc. Nuclear Thermal-Hydraulics, ANS 1990 Winter Meeting, Washington, D.C., 313, November 1990.

Chiang, J.H., Aritomi, M., Inoue R., and Mori, M., "Thermohydraulics During Startup in Natural Circulation Boiling Water Reactors", NURETH-5, September 1992.

Ineda F., and Yasuo, Y., "The Boiling Flow Instability of a Natural Circulation BWR with a Chimney at Low Pressure Startup", Proceedings of the International Conference on Design and Safety of Advanced Nuclear Power Plants, Volume 3, October 1992.

Nissen, W.H.M., Voet, J.van der, and Karuza, J., "The Startup of the Dodewaard Natural Circulation BWR - Experiences", Proceedings of the International Conference on Design & Safety of Advanced Nuclear Power Plants, Vol. 3, October 1992.

Rohatgi, U.S., et al., "RAMONA-4B - A Computer Code With Three-Dimensional Neutron Kinetics for BWR and SBWR System Transients", NUREG/CR number to be published, BNL-NUREG number to be published, March 1994.

Wulff, W., et. al., "A Description and Assessment of RAMONA-3B MOD.O CYCLE 4: A Computer Code with Three-Dimensional Neutron Kinetics for BWR System Transients", NUREG/CR-3664, BNL-NUREG-51746, BNL, 1984.

7.0 APPENDIX A

RAMONA-4B Thermal Hydraulic Governing Equations

Vapor Mass Balance Equation

$$\frac{\partial}{\partial t}(\alpha\rho_g) + \nabla \cdot (\vec{j}_g\rho_g) = \Gamma_v \qquad (1)$$

Liquid Mass Balance Equation

$$\frac{\partial}{\partial t}\left[(1-\alpha)\,\rho_l \right] + \nabla \cdot (\vec{j}_l\rho_l) = -\Gamma_v \qquad (2)$$

where the α, ρ, j_g and j large void fraction, density, and volumetric fluxes of vapor and liquid, respectively. Since the vapor phase is assumed to be saturated, Equation 1 can provide void fraction directly. The right hand terms in Equations 1 and 2 represent the net vapor generation from wall heat transfer and in the bulk. Constitutive relations are used to account for these terms. During normal operation subcooled boiling occurs in the lower part of the core, while nucleate pool boiling prevails over the entire height of the rod bundle. Post CHF heat transfer is of importance only in the case of dryout. Appropriate models for wall heat transfer are selected by the thermal hydraulics model in response to the heat input from the neutronics calculations. Volumetric fluxes of vapor and liquid are given by:

$$\vec{j}_g = \alpha\vec{v}_g \qquad and \qquad \vec{j}_l = (1-\alpha)\vec{v}_l$$

Expanding the left hand sides of Equations 1 and 2, and adding them, the divergence of mixture volumetric flux is obtained:

$$\nabla \cdot \vec{j}_m = (\rho_l - \rho_g)\frac{\Gamma_v}{(\rho_l\,\rho_g)} - \left[\frac{\alpha}{\rho_g}\frac{D_g\rho_g}{Dt} + \frac{(1-\alpha)}{\rho_l}\frac{D_l\rho_l}{Dt}\right] \qquad (3)$$

where $j_m = j_g + j_l$, and D/Dt represents convective derivative for phases I = g or l. The first term on the right hand side corresponds to the total change in volume associated with generation of vapor. The terms within the square brackets account for the compressibilities of the vapor and liquid phase, respectively. Since the vapor is assumed to be at a saturated state at all times, the vapor compressibility term is a function of the pressure only. Therefore, this is represented by the equations of state and the variation of pressure. On the other hand, the liquid phase can be subcooled, saturated or superheated, hence the density is dependent on the specific internal energy and the system pressure. Expanding the second term on the right hand side of Equation 3 and using the equations of state, a governing equation for pressure variation can be obtained. The calculated pressure represents the average system pressure of the reactor pressure vessel.

System Pressure Equation

In RAMONA-4B, an ordinary differential equation for a single pressure is generated by integrating this pressure equation over the volume of the entire reactor pressure vessel:

$$\dot{p} = \frac{W_{fw} + W_{l,ic} + W_{boron} - W_{STEAM} - W_{s,ic} + W_{\Gamma_v} + W_{expan}^{core}}{\int_{Vessel}\left[\frac{\alpha}{\rho_g}\frac{d\rho_g}{dp} + \frac{(1-\alpha)}{\rho_l}\left(\frac{\partial\rho_l}{\partial p}\right)_u\right]dV} \qquad (4)$$

The numerator of Equation 4 is the sum of the volumetric flow rates of the fluids crossing the boundary of region of integration, which is the surface of the reactor pressure vessel, such as, feed water flow, condensate return from isolation condensers, the poison boron

solution from the standby liquid cooling system, steam flow, and steam flow into the isolation condensers. The other terms relate to vapor generation and thermal expansion in the core. The denominator of Equation 4 represents the compressibilities of the two phases within the entire pressure vessel. Integration of this equation provides the instantaneous pressure within the reactor pressure vessel (RPV). Thermophysical properties of the two phases are calculated with this pressure. This procedure of decoupling the pressure to an independent form significantly improves the computational efficiency of RAMONA-4B. Next, we discuss the momentum balance in the RPV.

Mixture Momentum Balance Equation

$$\frac{\partial G_m}{\partial t} + \frac{\partial}{\partial z}\left[\alpha\rho_g w_g^2 + (1-\alpha)\rho_l w_l^2 \right] = -\frac{\partial p}{\partial z} - g_z\rho_m - f_l \Phi_l^2 \frac{G_m|G_m|}{2\rho_l d_h} \tag{5}$$

Mixture Mass Flux

$$G_m = \alpha\rho_g w_g + (1-\alpha)\rho_l w_l \tag{6}$$

Mixture Density

$$\rho_m = \alpha\ \rho_g + (1-\alpha)\ \rho_l \tag{7}$$

In RAMONA-4B, closed loop or contour momentum equations for each of the thermal hydraulic channels is derived by integrating Equation 5 over closed flow loops. Therefore, the mass flux G_m is solved for each hydraulic channel. Iterations are performed on the sum of the mass fluxes of these channels for the total pressure drop from core inlet through upper plenum and riser of the pressure vessel. Constitutive relations for single phase friction factor, f, and two phase multiplier, φ_l, are used to solve the closed loop momentum equation.

Mixture Energy Balance Equation

$$\frac{\partial}{\partial t}\left[\alpha\rho_g u_g + (1-\alpha)\rho_l u_l \right] + \frac{\partial}{\partial z}\left[\alpha\rho_g h_g w_g + (1-\alpha)\rho_l h_l w_l \right] = \frac{q_w}{A} + q_l(1-\alpha) \tag{8}$$

In this equation, the first term on the right hand side is the wall heat transfer and the second is the direct heating of the liquid due to gamma ray attenuation and neutrons slowing down. In this equation A, u, and h represent the cross-sectional flow area for heat transfer, phasic internal energy and enthalpy, respectively. Since the vapor is assumed to be in a saturated state, once the pressure, void fraction and the right hand terms are known, this equation is used to calculate the nonequilibrium internal energy of the liquid only. Consequently the temperature of the liquid is obtained.

Constitutive Relations for Thermal Hydraulic Models

A detailed description of the constitutive relations for convective heat transfer from the wall to the liquid is given by Wulff, et al., (1984) and Rohatgi, et al., (1994). The following principal models and correlations are required:

- Non Equilibrium Vapor Generation and Condensation
- Single and Two Phase Wall Friction
- Wall Heat Transfer
- Flow Dependent Loss Coefficients
- Drift Flux Model

Vapor Generation and Condensation Model

Vapor generation and condensation model is briefly described here. The RAMONA-4B code is designed to account for thermal nonequilibrium to the extent that the liquid phase in the two-phase mixture is allowed to be subcooled, saturated, or superheated while the vapor phase is restricted to saturation conditions. The temperature of the liquid in the two-phase mixture is entirely dictated by the calculation for the nonequilibrium vapor generation rate. The vapor generation rate has a strong and direct impact on the predictions of vapor voids and, therefore, on reactivity feedback and power generation.

The vapor generation model in RAMONA-4B is an empirical correlation that is based on FRIGG tests. The current constants of the vapor generation in the code were obtained from experimental data in earlier versions of RAMONA with slip model. The vapor generation rate is computed in two parts:

$$\Gamma_v = \Gamma_w + \Gamma_{ph} \tag{9}$$

The first part accounts for evaporation due to heat transfer from the wall to the liquid phase. The second part accounts for mass transfer (evaporation or condensation) due to heat transfer between the phases. The interfacial mass transfer, represented by the second term on the right-hand side of the above equation, is:

$$\Gamma_{ph} = \frac{C_{11} + C_{12}\,\alpha(1-\alpha)}{h_{fg}}[(t_l - t_{sat}) + C_{13}|t_l - t_{sat}|] \tag{10}$$

where α, t_{sat}, h_{fg}, and t_l are the void fraction, saturation temperature, latent heat of vaporization and the liquid temperature, respectively. The parameters C_{11}, C_{12}, and C_{13} are user-specified values from experimental test data. The equation above produces condensation when liquid temperature is less than saturation temperature and evaporation otherwise. The parameter C_{13} is a value between 0 and 1 and measures the retardation or lagging between evaporation and condensation. As $\alpha(1-\alpha)$ is proportional to the interfacial area density, the parameter C_{12} can control the interfacial mass transfer rate due to interfacial heat transfer. The parameter C_{11} prescribes the onset of boiling.. As mentioned before, the mass transfer equation above is not a mechanistic model. There exists no universal set of parameters that can represent all possible conditions in a BWR reactor core (Wulff, 1984). The three parameters C_{11}, C_{12}, and C_{13} have, and can be expected, to provide the empirical equation sufficient freedom of adjustment to fit any steady-state experimental data. The model performs less reliably during pressure fluctuations such as experienced in flashing and recondensing (Wulff, 1984). The model produces unrealistically high liquid superheating under steady-state boiling at high void fractions. It is not possible to produce equilibrium phase change under conditions, such as adiabatic flow with pressure oscillations of low frequency, where equilibrium conditions have been observed (Wulff, 1984). The effect of increasing the C_{11} parameter by a factor of ten is shown below below in Figure A1. The result is a uniform increase for all void fractions.

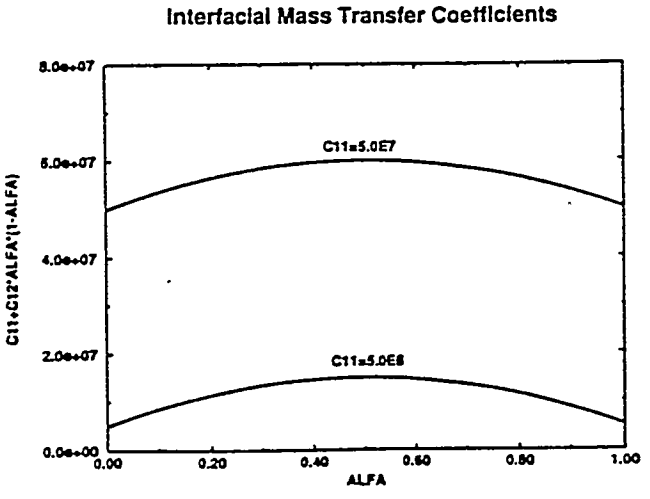

Fig. A1. Bulk Vapor Generation Coefficients

RAMONA-4B can be used for non-reactor applications such as simulation of thermal hydraulic experiments conducted in facilities with electrically heated test sections. In these applications, power applied to the test section is specified as an input. The test facility to be simulated should include a downcomer, lower plenum, core, riser, and a steam dome. The reactor vessel is always represented by seven components. The list of components starting from the upper part of the downcomer region is listed as:

1. Downcomer 1
2. Downcomer 2
3. Lower Plenum 1
4. Lower Plenum 2
5. Core
6. Riser
7. Steam Dome

All the above components are one-dimensional; the Core component consists of a number of parallel channels, specified as an input by the user, connecting the Lower Plenum 2 and the Riser. The Riser component consists of the combination of upper plenum, chimney, and steam separator regions. Downcomer 1 is followed by Downcomer 2 which represents the inner region of the jet pumps geometrically (Wulff, 1984). With the exception of the Lower Plenum 1, all vessel components are vertical and with constant flow areas. However, the flow areas for all components are different.

TABLE I

RAMONA-4B Input Deck for Aritomi's Experiment							
Component	Downcomer 1	Downcomer 2	Lower Plenum 1	Lower Plenum 2	Core	Riser	Dome
No. of nodes	6	6	2	3	24	5	1
Height (m)	2.430	1.830	1.310	1.165	1.670	1.495	0.600
Flow Area (m^2)	0.00073	0.00073	0.0011	0.0380	0.00016	0.0579	0.1257
Hydraulic Diameter (m)	.0283	.0283	.0283	0.2620	0.0096	0.2715	0.4000

TABLE II

RAMONA-4B 2 PARALLEL CHANNEL MODEL SYMMETRIC POWER DISTRIBUTION		
Time (sec)	*Cell Number*	*Evaporation/Condensation Rate* $(\frac{kg}{m^3 sec})$
4.00	*Channel 1 Exit (k=71)*	*0.4651E-10*
	Channel 2 Exit (k=72)	*0.4651E-10*
	Riser, Inlet (k=74)	*-0.1294E-02*
	Riser (k=75)	*-0.1261E-07*
19.00	*Channel 1 Exit (k=71)*	*0.2256E-08*
	Channel 2 Exit (k=72)	*0.2256E-08*
	Riser, Inlet (k=74)	*-0.1739E-03*
	Riser (k=75)	*-0.1454E-15*

TABLE III

RAMONA-4B 2 PARALLEL CHANNEL MODEL ASYMMETRIC POWER DISTRIBUTION ENHANCED VAPOR-GENERATION MODEL		
Time (sec)	*Cell Number*	*Evaporation/Condensation Rate* $(\frac{kg}{m^3 sec})$
4.00	*Channel 1 Exit (k=71)*	*0.1456E-05*
	Channel 2 Exit (k=72)	*0.3236E-04*
	Riser, Inlet (k=74)	*-0.1571E-02*
	Riser, Inlet (k=75)	*-0.1066E-07*
62.00	*Channel 1 Exit (k=71)*	*0.1163E-07*
	Channel 2 Exit (k=72)	*0.3141E-13*
	Riser, Inlet (k=74)	*-0.2509E-03*
	Riser, Inlet (k=75)	*-0.8028E-48*

TABLE IV

RAMONA-4B 2 PARALLEL CHANNEL MODEL ASYMMETRIC POWER DISTRIBUTION ENHANCED VAPOR-GENERATION MODEL		
Time (sec)	*Cell Number*	*Evaporation/Condensation Rate* $(\frac{kg}{m^3 sec})$
4.00	*Channel 1 Exit (k=69)*	*0.8916E-11*
	Channel 2 Exit (k=70)	*0.4250E-11*
	Riser Inlet 1 (k=71)	*-0.7500E-03*
	Riser Inlet 2 (k=72)	*-0.6751E-03*
	Riser (k=74)	*-0.5009E-08*
19.00	*Channel 1 Exit (k=71)*	*0.3479E-07*
	Channel 2 Exit (k=72)	*-0.3834E-12*

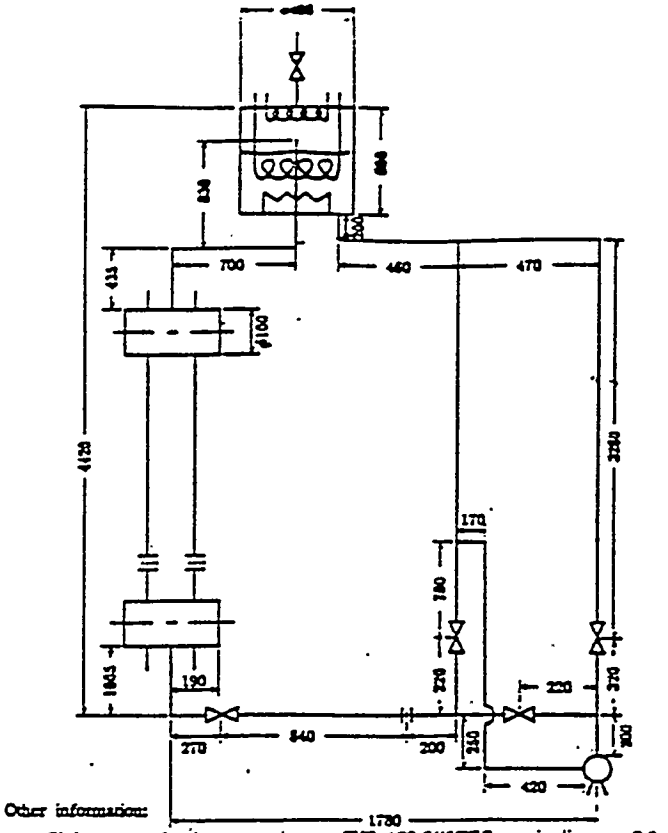

Other information:

Piping except for the test section are SUS A20 3/4"(27.2 mm in diameter, 2.8 mm in thickness).

Ball Valves(pt 3/4", d=16mm) are used to control flow rate.

Pump is the centrifugal type 1 1/4"(d=32mm).

Pump performance is head[m]/flow rate[liter/min] — 4/130, 6/104, 8/65.

Inner diameter for orifices used in the channels are 12 mm and for orifice used in the loop is 13mm.

Fig. 1. Aritomi's experimental apparatus.

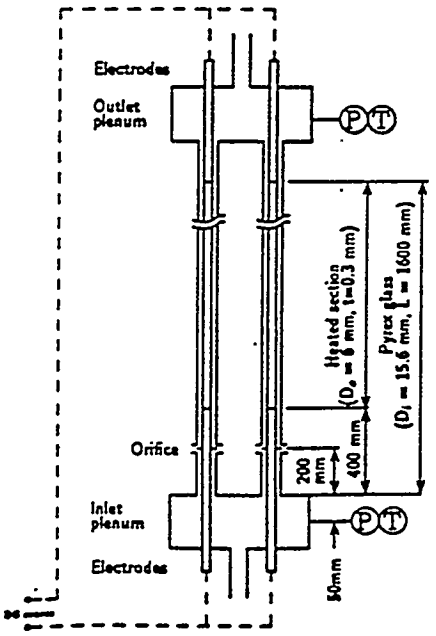

Fig. 2. Test section with heated parallel channels.

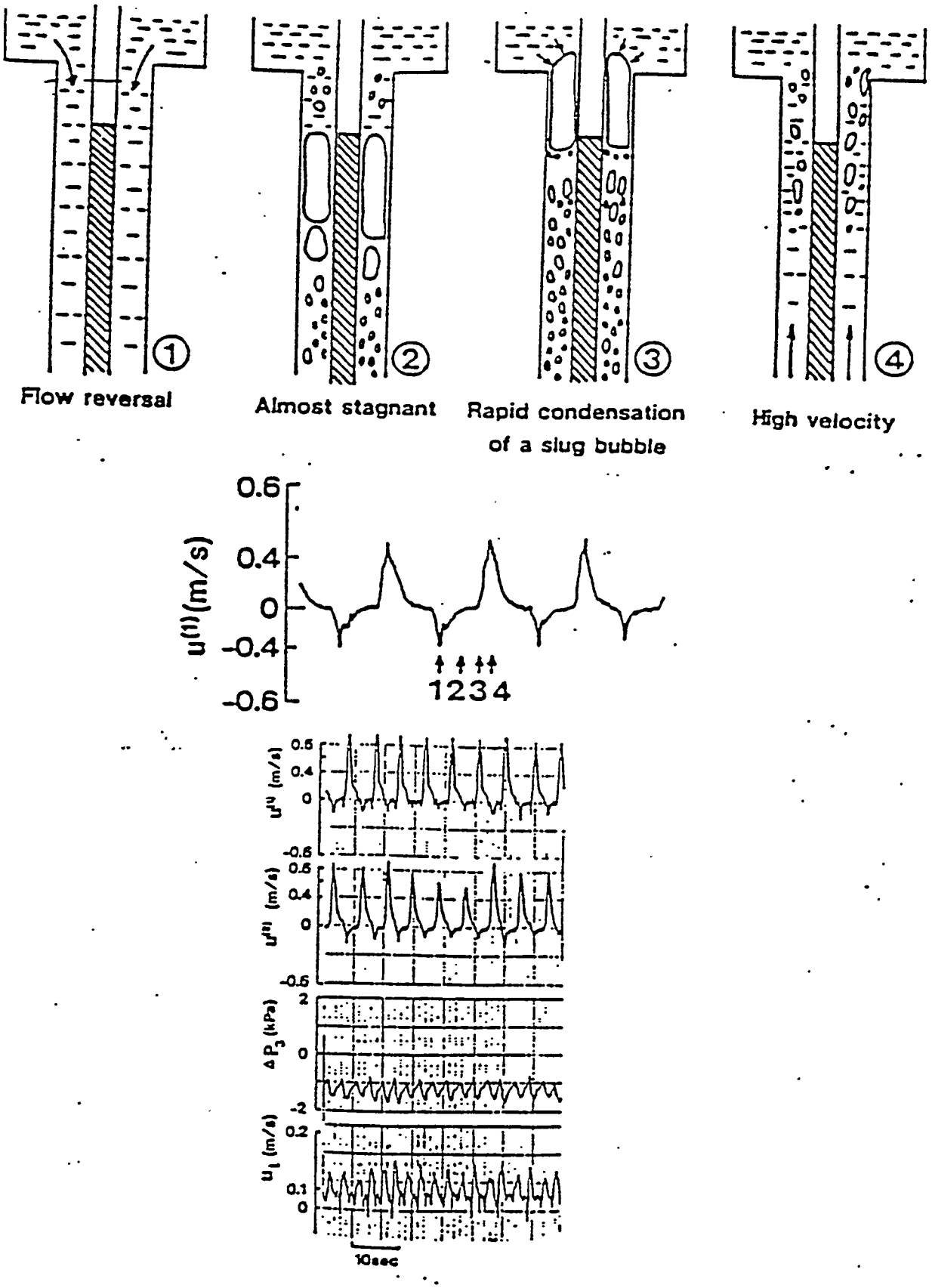

Fig. 3. Geysering instability (from Aritomi (1993)).

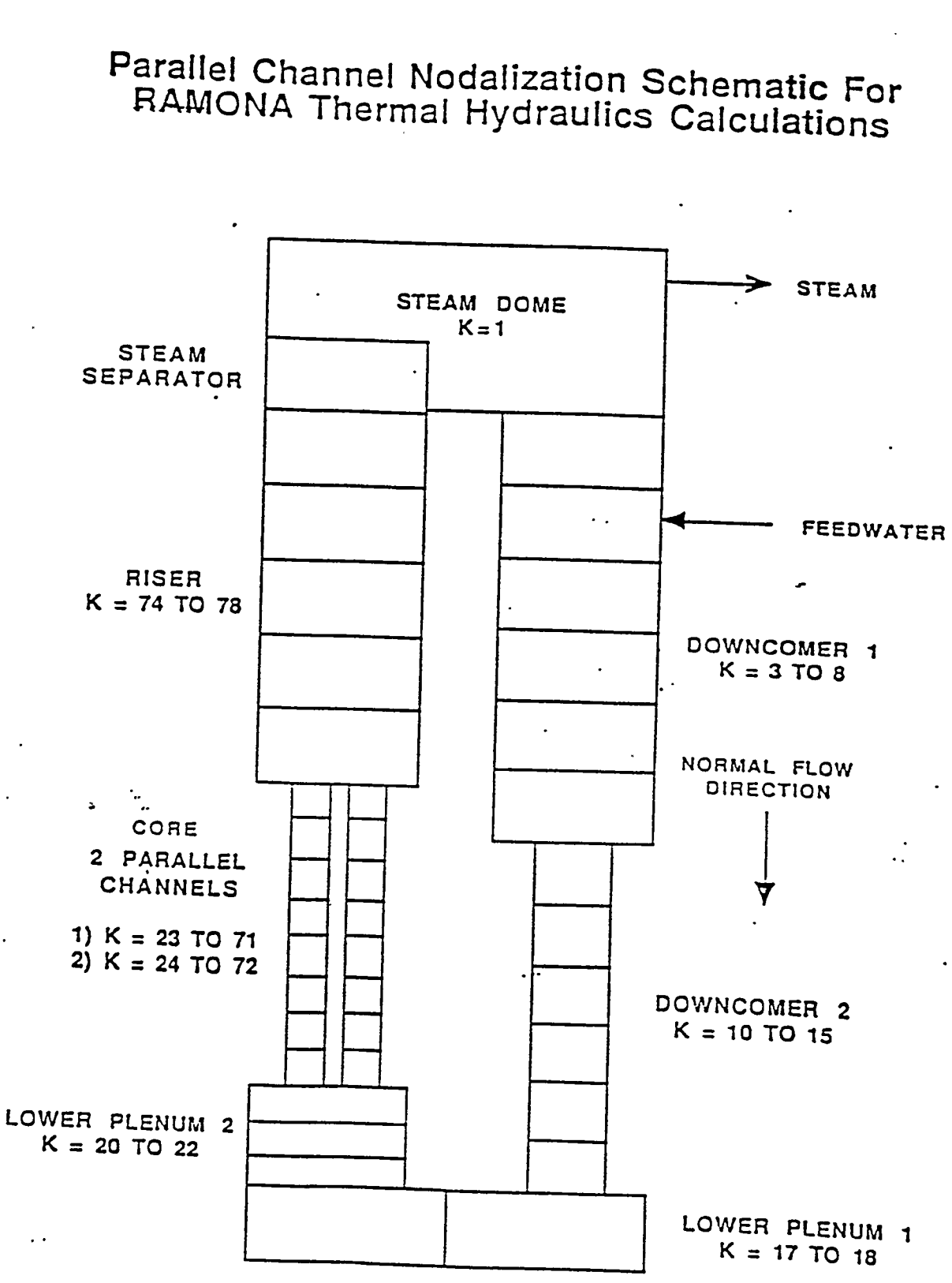

Fig. 4. RAMONA4B nodalization scheme.

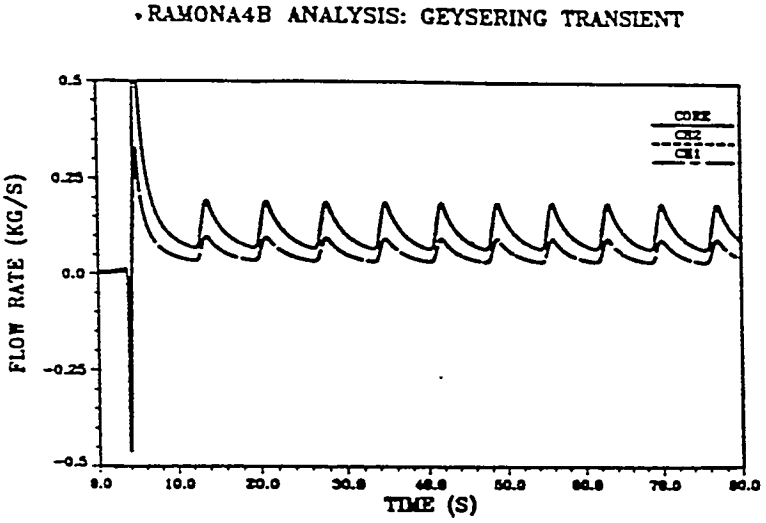

Fig. 5. Channel 1, channel 2, and total core inlet mass flowrate.

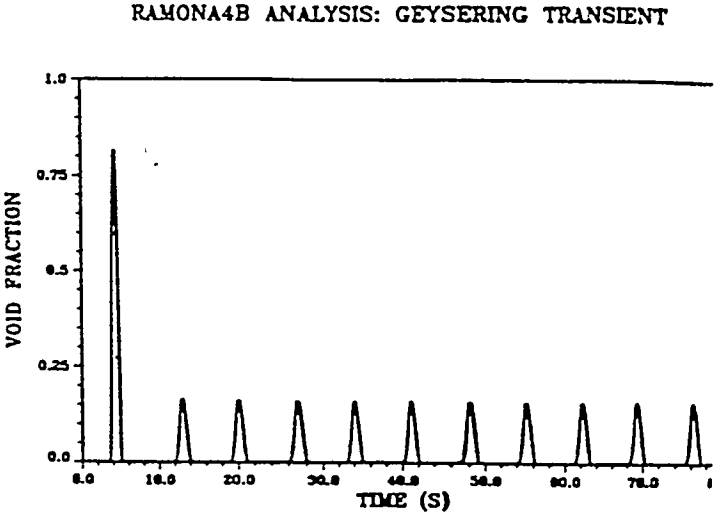

Fig. 6. Core average void fraction.

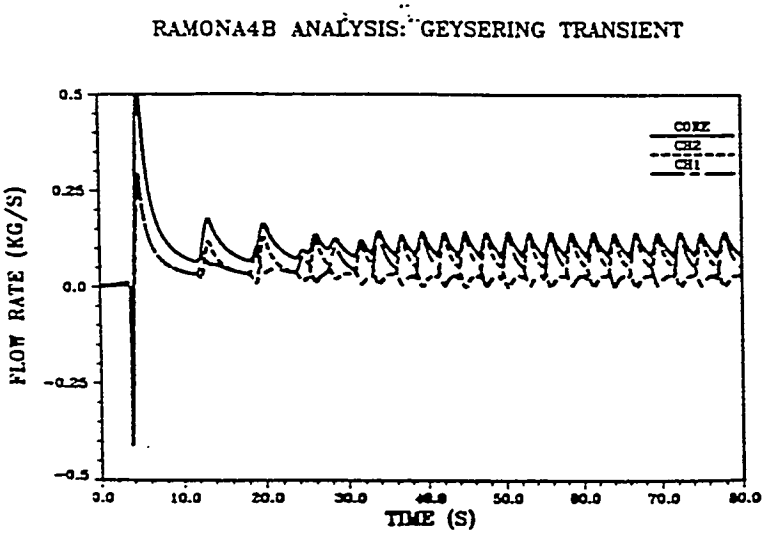

Fig. 7. Channel 1, channel 2, and total core inlet mass flowrate.

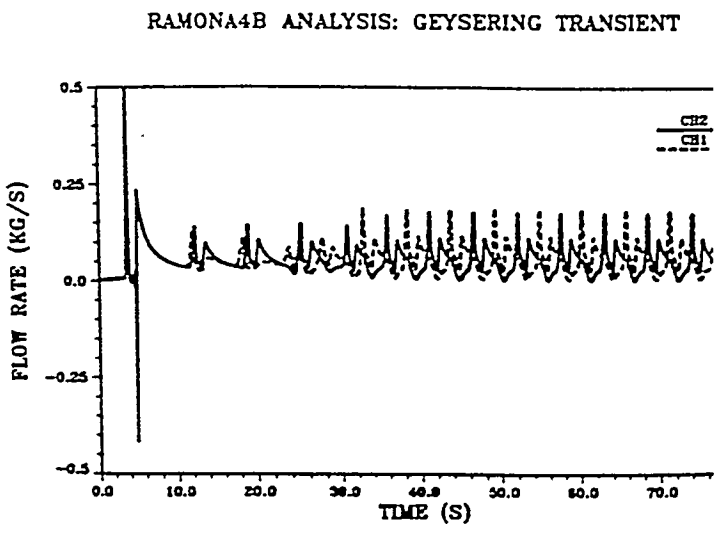

Fig. 8. Channel 1 and channel 2 exit mass flowrate.

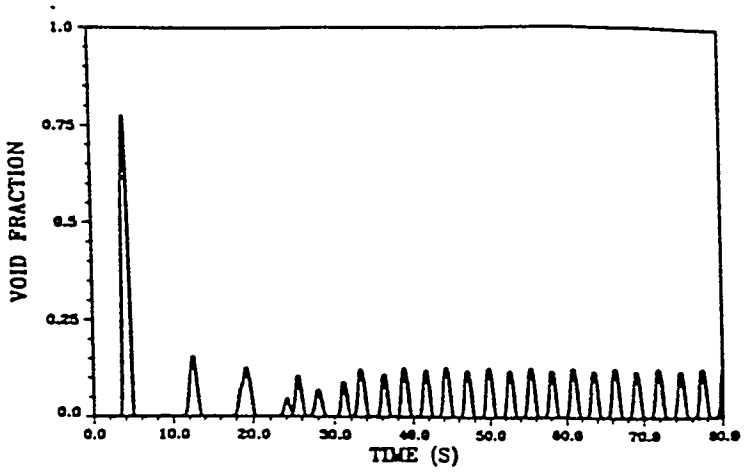

Fig. 9. Core average void fraction.

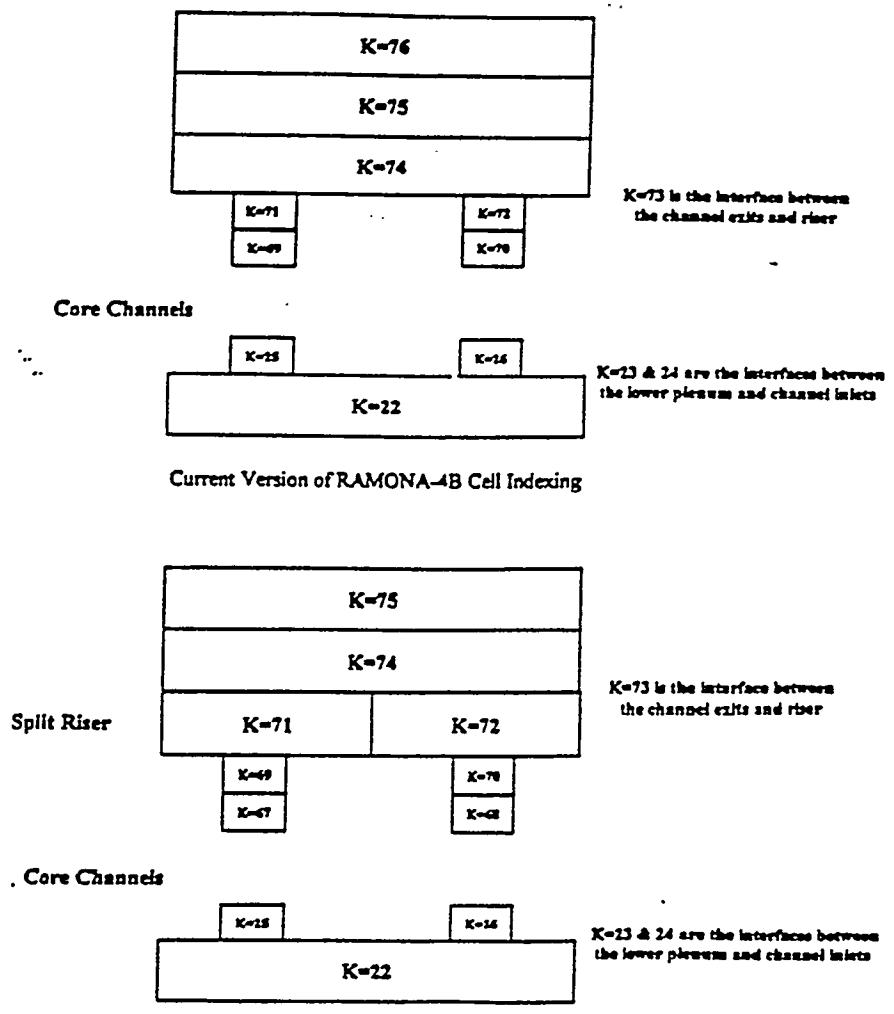

Fig. 10. Current and modified versions of RAMONA4B cell indexing.

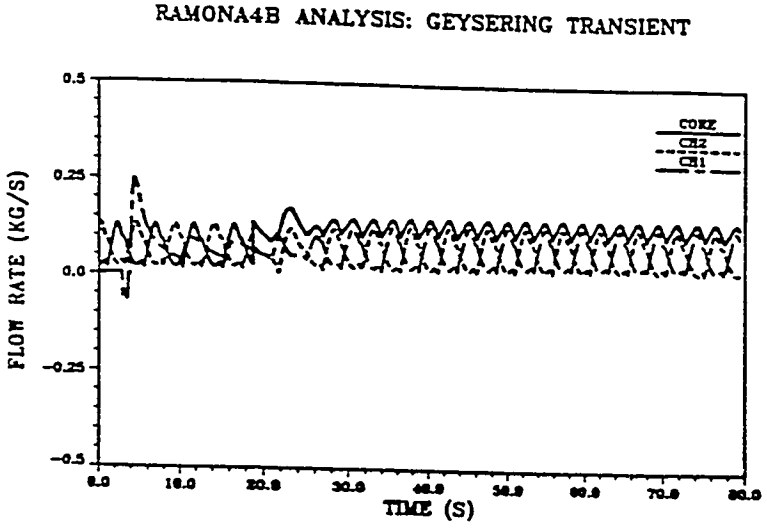

Fig. 11. Channel 1, channel 2, and total core inlet mass flowrate.

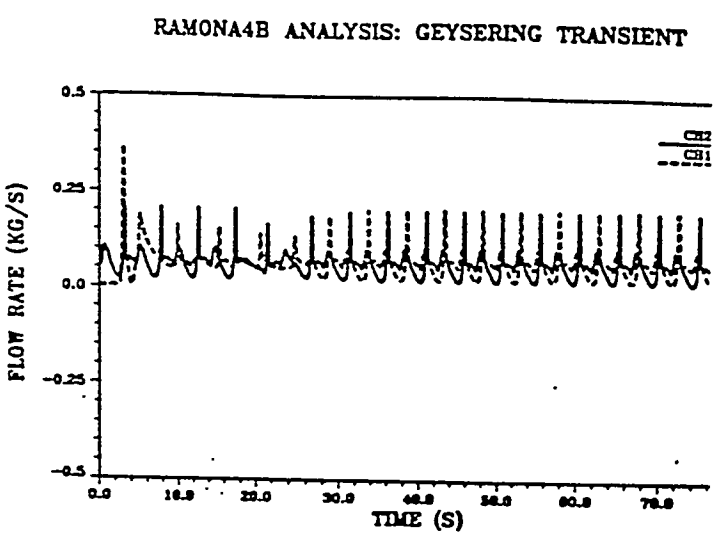

Fig. 12. Channel 1 and channel 2 exit mass flowrate.

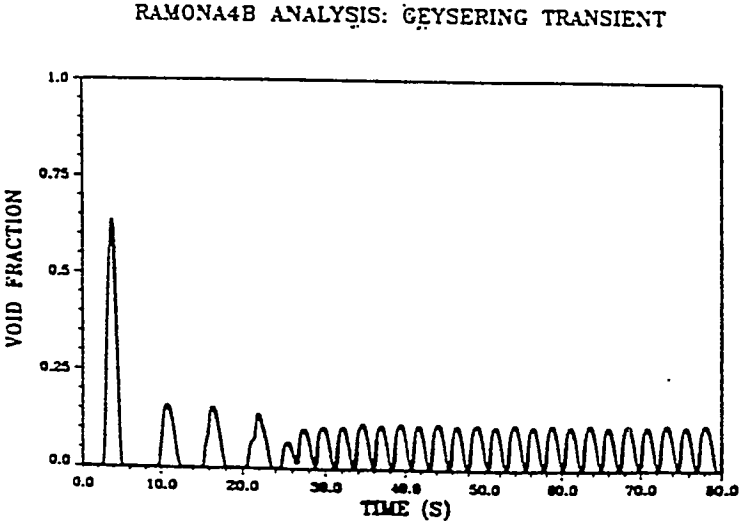

Fig. 13. Core average void fraction.

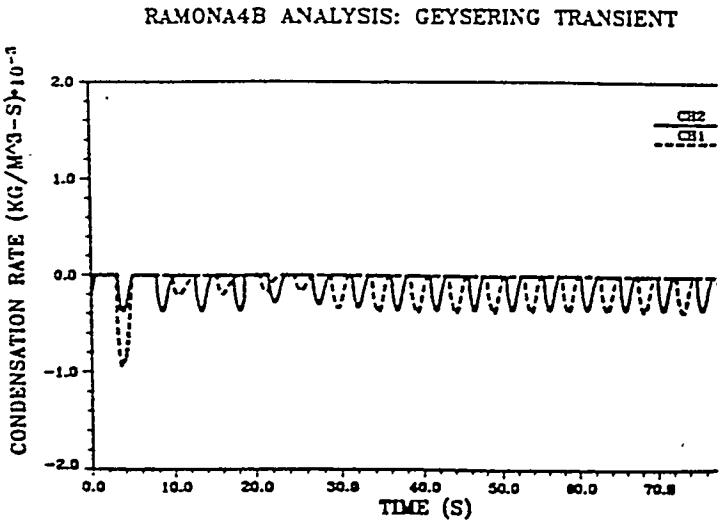

Fig. 14. Channel 1 and channel 2 exit condensation rates.

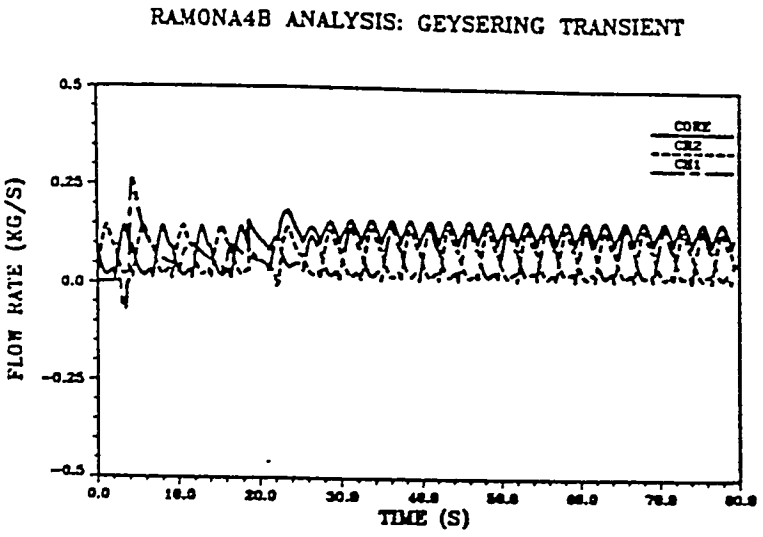

Fig. 15. Channel 1, channel 2, and total core inlet mass flowrate.

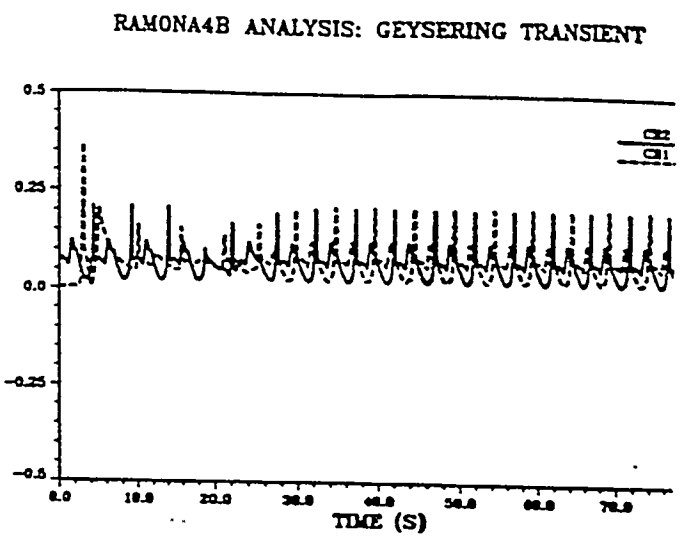

Fig. 16. Channel 1 and channel 2 exit mass flowrate.

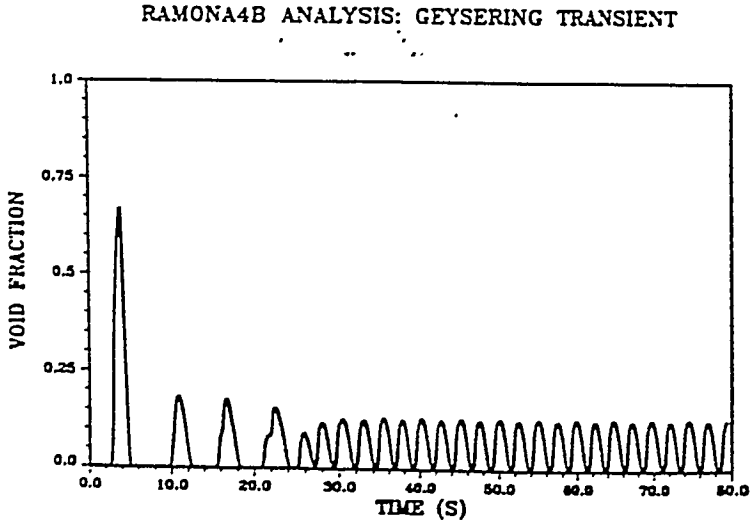

Fig. 17. Core average void fraction.

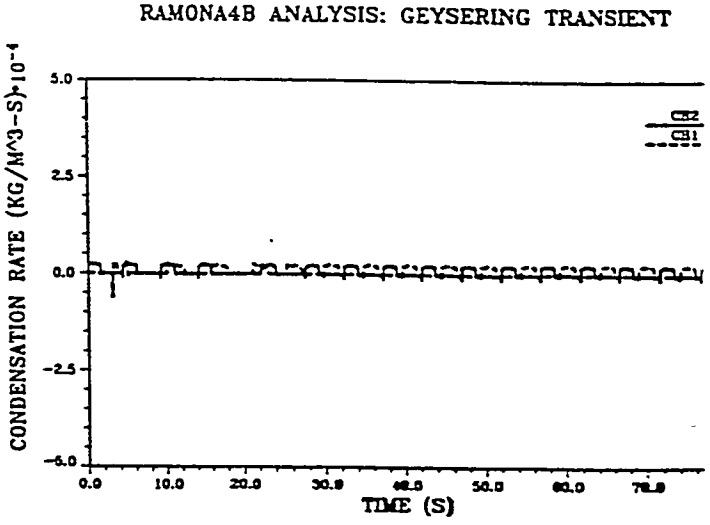

Fig. 18. Channel 1 and channel 2 exit condensation rate

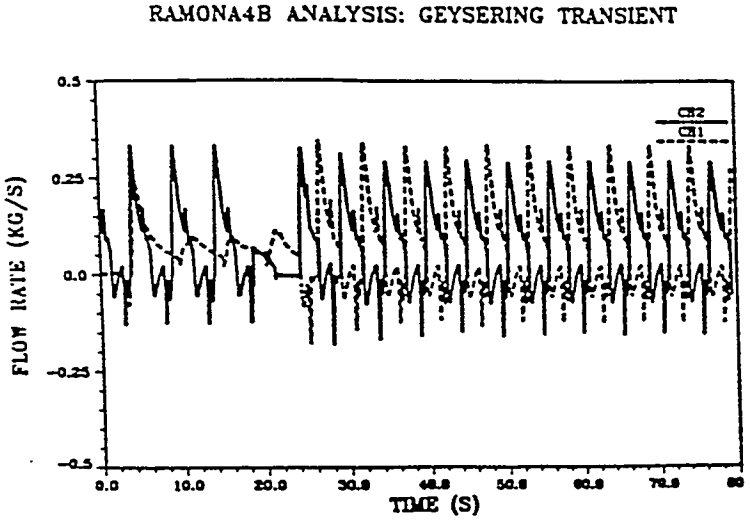

Fig. 19. Channel 1 and channel 2 inlet mass flowrates.

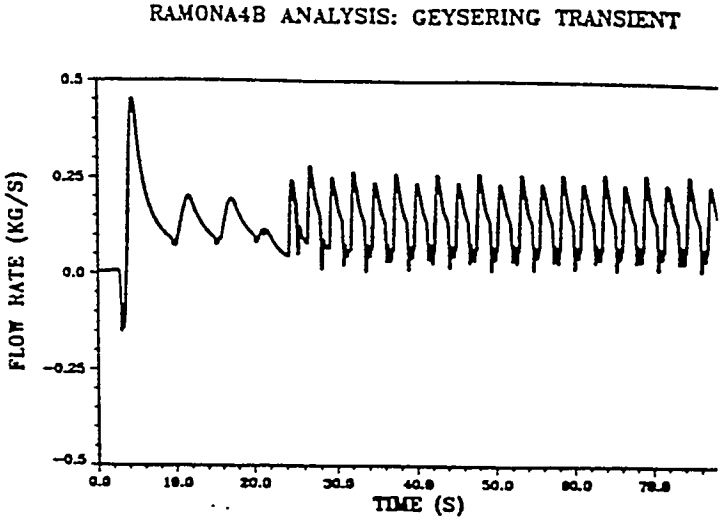

Fig. 20. Total core inlet mass flowrate.

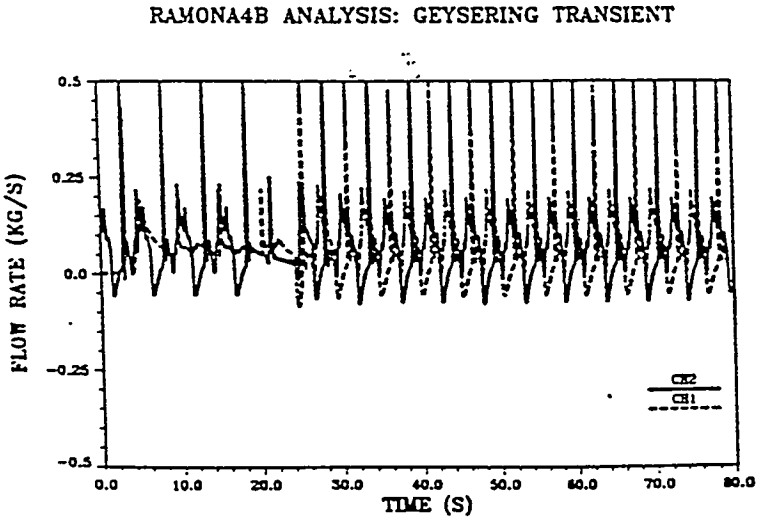

Fig. 21. Channel 1 and channel 2 exit mass flowrates.

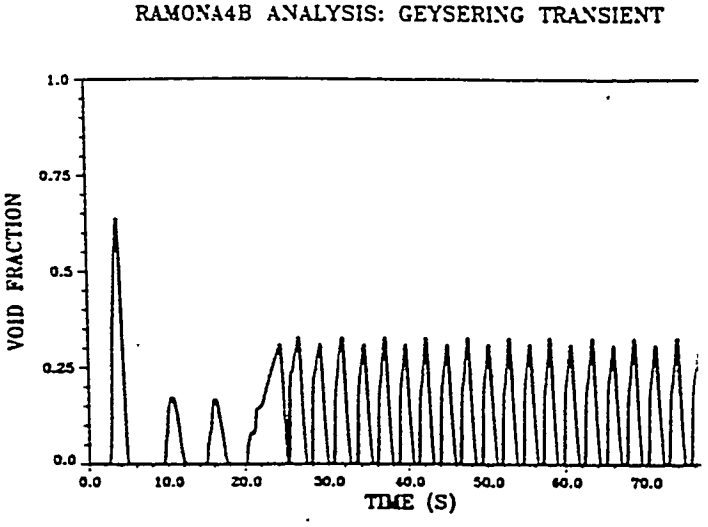

Fig. 22. Core average void fraction.

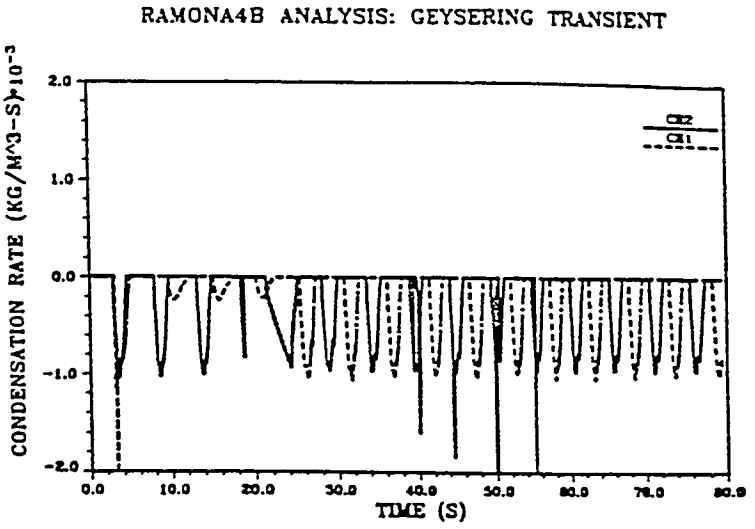

Fig. 23. Channel 1 and channel 2 exit condensation rates.

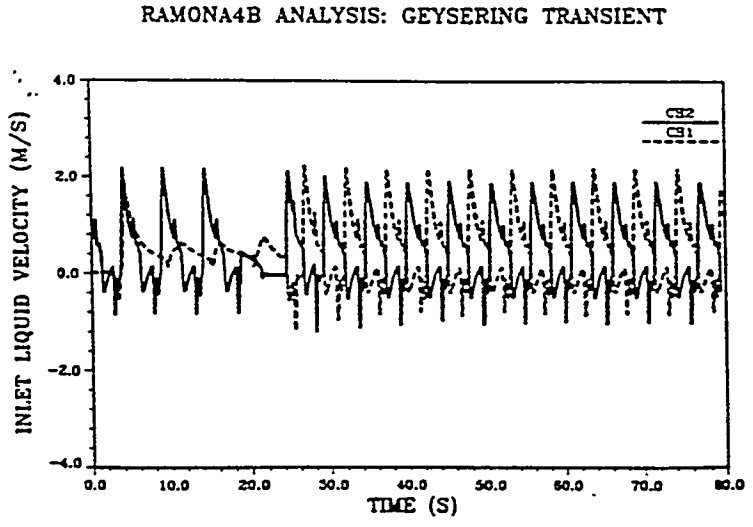

Fig. 24. Channel 1 and channel 2 inlet liquid velocities.

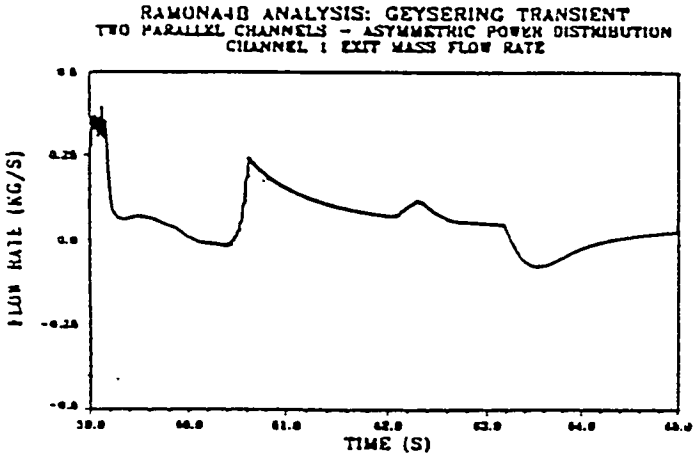

Channel 1 Exit Mass Flow

(a)

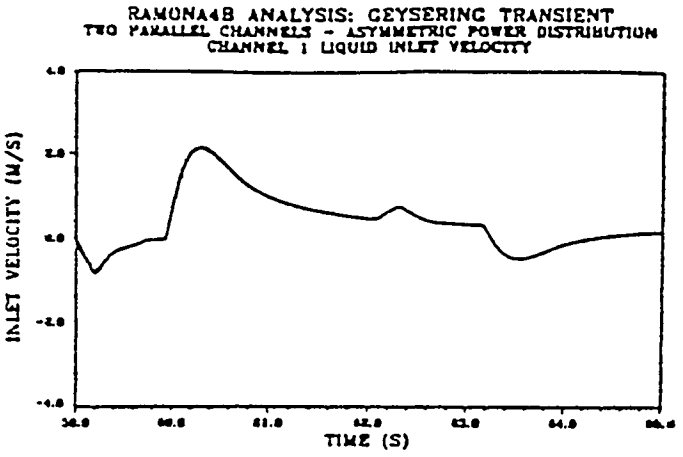

Channel 1 Liquid Inlet Velocity

(b)

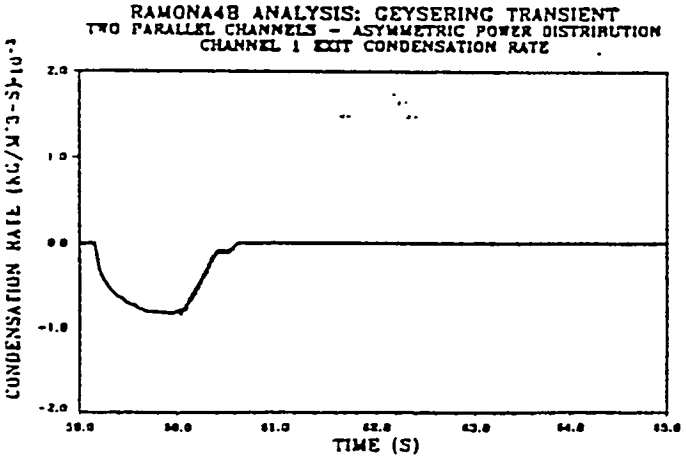

Channel 1 Exit Condensation Rate

(c)

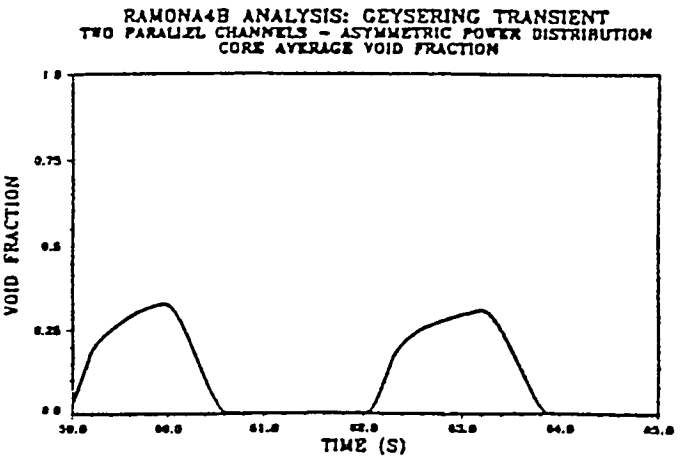

Core Average Void Fraction

(d)

Fig. 25. Modified RAMONA4B with enhanced vapor generation model.

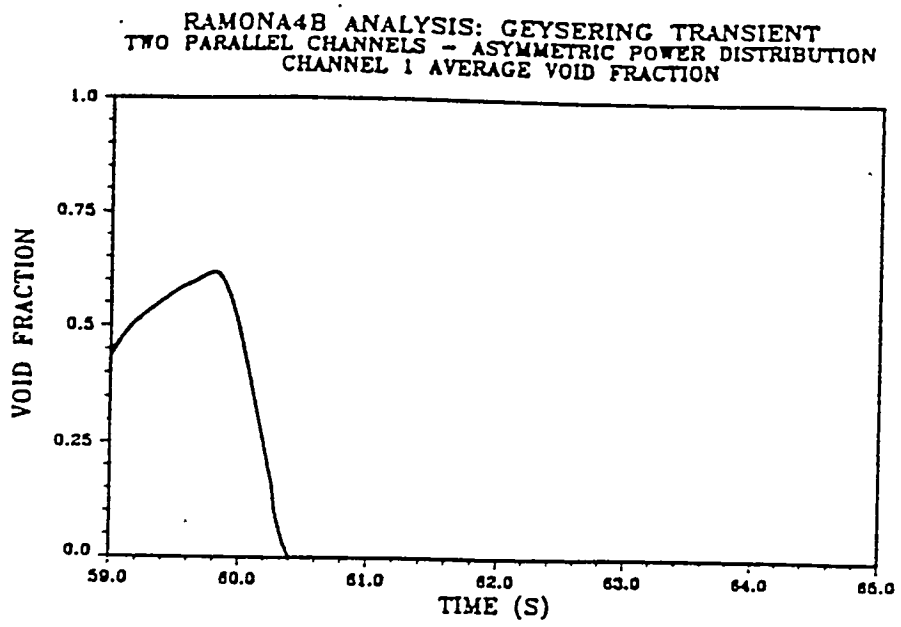

Channel 1 Average Void Fraction

(e)

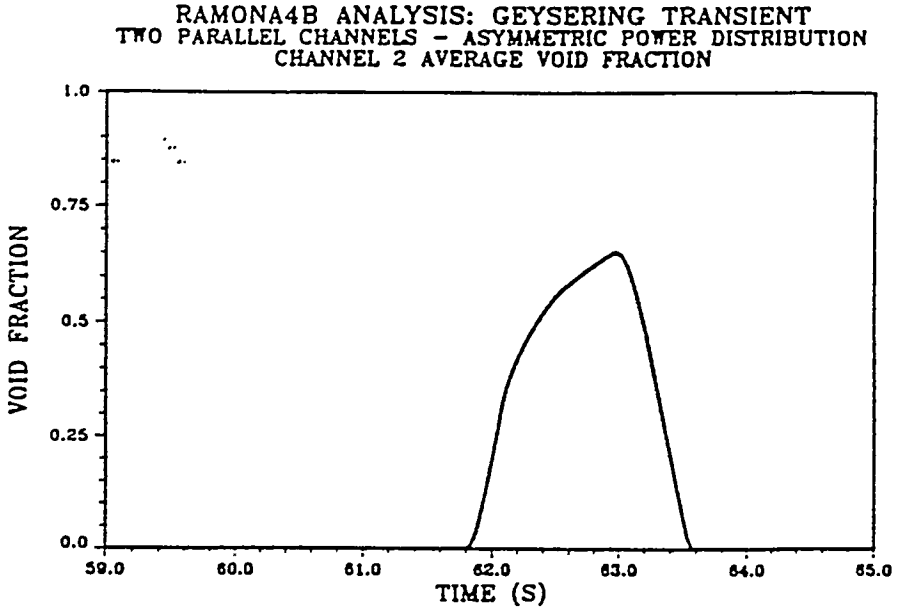

Channel 2 Average Void Fraction

(f)

Fig. 25. Modified RAMONA4B with enhanced vapor generation model (Cont'd).

1. Flow reversal due to sudden vapor generation in channel 1.

2. Condensation of large bubbles at channel 1 exit outlet produces large increase in channel flow. Peak velocity amplitude reached after initiation of subcooling restoration in channel 1 due to flow inertia. Flow begins to decrease thereafter as the subcooled condition is being restored.

3. Momentary flow "spike" due to flow reversal at inlet in channel 2 from sudden vapor generation in that channel. Flow continues decreasing afterwards.

4. Condensation of large bubbles at exit of other parallel channel, channel 2, causes flow reversal in this channel, channel 1. This is due to the exit condensation rate being greater than the overall natural circulation rate of the system. Flow then begins to increase subsequently due to bouyancy effects of the liquid heated in the channel. Cycle is repeated.

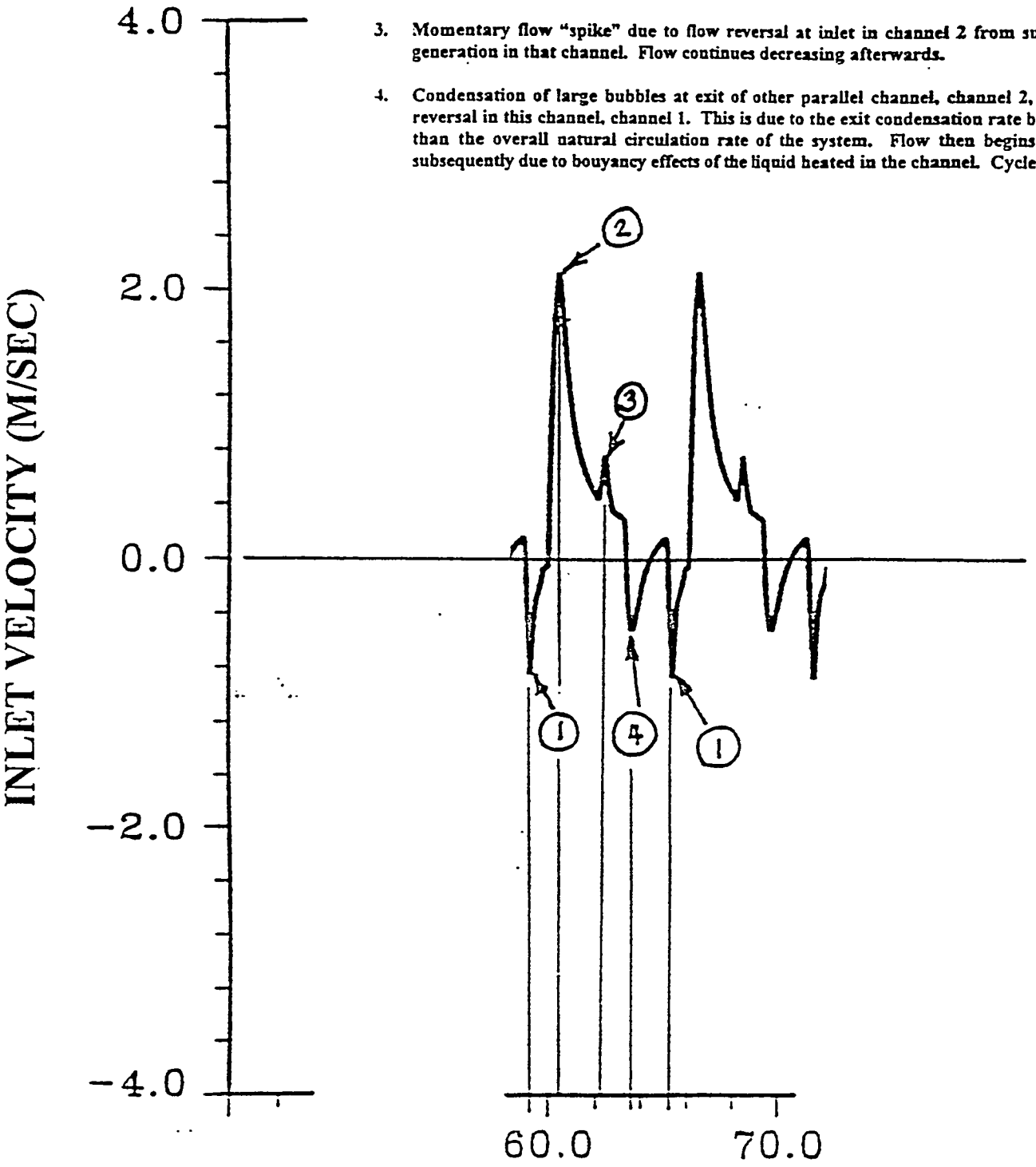

Fig. 26. Channel 1 inlet velocity from t = 59 to t = 65 seconds.